Eur J Nucl Med Mol Imaging (2011) 38:108–119
DOI 10.1007/s00259-010-1597-8

ORIGINAL ARTICLE

Development of new folate-based PET radiotracers: preclinical evaluation of ^{68}Ga-DOTA-folate conjugates

Melpomeni Fani · Xuejuan Wang · Guillaume Nicolas · Christelle Medina · Isabelle Raynal · Marc Port · Helmut R. Maecke

Received: 18 May 2010 / Accepted: 6 August 2010 / Published online: 27 August 2010

Abstract
Purpose A number of ^{111}In- and ^{99m}Tc-folate-based tracers have been evaluated as diagnostic agents for imaging folate receptor (FR)-positive tumours. A ^{68}Ga-folate-based radiopharmaceutical would be of great interest, combining the advantages of PET technology and the availability of ^{68}Ga from a generator. The aim of the study was to develop a new ^{68}Ga-folate-based PET radiotracer.
Methods Two new DOTA-folate conjugates, named P3026 and P1254, were synthesized using the 1,2-diaminoethane and 3-{2-[2-(3-amino-propoxy)-ethoxy]-ethoxy}-propylamine as a spacer, respectively. Both conjugates were labelled with $^{67/68}$Ga. Binding affinity, internalization and externalization studies were performed using the FR-positive KB cell line. Biodistribution and PET/CT imaging studies were performed in nude mice, on a folate-deficient diet, bearing KB and HT1080 (FR-negative) tumours, concurrently. The new radiotracers were evaluated comparatively to the reference molecule ^{111}In-DTPA-folate (^{111}In-P3139).
Results The K_d values of $^{67/68}$Ga-P3026 (4.65±0.82 nM) and $^{67/68}$Ga-P1254 (4.27±0.42 nM) showed high affinity for the FR. The internalization rate followed the order $^{67/68}$Ga-P3026>$^{67/68}$Ga-P1254>^{111}In-P3139, while almost double cellular retention was found for $^{67/68}$Ga-P3026 and $^{67/68}$Ga-P1254, compared to ^{111}In-P3139. The biodistribution data of $^{67/68}$Ga-DOTA-folates showed high and receptor-mediated uptake on the FR-positive tumours and kidneys, with no significant differences compared to ^{111}In-P3139. PET/CT images, performed with ^{68}Ga-P3026, showed high uptake in the kidneys and clear visualization of the FR-positive tumours.
Conclusion The DOTA-folate conjugates can be efficiently labelled with ^{68}Ga in labelling yields and specific activities which allow clinical application. The characteristics of the $^{67/68}$Ga-DOTA-folates are comparable to ^{111}In-DTPA-folate, which has already been used in clinical trials, showing that the new conjugates are promising candidates as PET radiotracers for FR-positive tumours.

Keywords Folate receptor · DOTA-folate conjugates · ^{68}Ga · PET imaging

M. Fani · X. Wang · H. R. Maecke
Division of Radiological Chemistry, University Hospital Basel, 4031 Basel, Switzerland

G. Nicolas
Department of Nuclear Medicine, University Hospital Basel, 4031 Basel, Switzerland

C. Medina · I. Raynal · M. Port
Research Department, Guerbet, 93600 Aulnay-sous-Bois, France

Present Address:
M. Fani · H. R. Maecke (✉)
Clinic for Nuclear Medicine, University Hospital Freiburg, Hugstetterstrasse 55, 79106 Freiburg, Germany
e-mail: helmut.maecke@uniklinik-freiburg.de

Abbreviations

TFA	Trifluoroacetic acid
DCM	Dichloromethane
Fmoc	9-Fluorenylmethoxycarbonyl
tBu	*tert*-Butyl
NHS	*N*-Hydroxysuccinimide
DCC	Dicyclohexylcarbodiimine
DMSO	Dimethyl sulfoxide
EDCI	1-Ethyl-3-(3-dimethylaminopropyl) carbodiimide
HOBt	Hydroxybenzotriazole

$DOTA(tBu)_3$	2-(4,7,10-Tris(2-*tert*-butoxy-2-oxoethyl)-1,4,7,10-tetraazacyclododecan-1-yl) acetic acid
HEPES	4-(2-Hydroxyethyl)-1-piperazineethanesulfonic acid
BSA	Bovine serum albumin
PBS	Phosphate-buffered saline
FCS	Fetal calf serum

Introduction

Folates are important vitamins for cell division and replication, since they are involved as coenzymes in the synthesis of a number of amino acids as well as nucleic acids. Cellular folate transport can be mediated by the folate receptor (FR), a membrane-anchored protein which binds physiologic folates with high affinity in the low nanomolar level [1]. FRs are only scarcely expressed in most normal tissues, while elevated expression has frequently been observed in a wide variety of human cancers (e.g. breast, cervical, colorectal, renal and nasopharyngeal), including>90% of ovarian and endometrial carcinomas [2–5]. Thus, FR has been used as a target for selective delivery of drugs to these tumours, such as radiopharmaceuticals, MRI contrast agents, chemotherapeutic agents, antisense oligonucleotides, protein toxins and liposomes with entrapped drugs [6–9]. Once folate conjugates are bound to FR they are transported into the cell through receptor-mediated endocytosis [10, 11].

Most of the folate-based radiopharmaceuticals have been developed for single photon emission computed tomography (SPECT) imaging, labelled with ^{99m}Tc [12–18] or ^{111}In [19–21]. Among these radioconjugates ^{111}In-diethylenetriaminepentaacetic acid (DTPA)-folate, developed by Green et al. and Low et al., has been evaluated in patients suffering from ovarian cancer in a phase I/II study [22]. ^{111}In-DTPA-folate exhibited rapid target tissue uptake and non-target tissue clearance, which gives the possibility of image acquisition at early time points after injection, while differentiation between benign and malignant masses was possible in patients with suspected new disease. Despite the encouraging results of the study more attention was paid to the development of ^{99m}Tc-labelled folate conjugates mainly because of the short half-life of ^{99m}Tc ($T_{1/2}$=6 h), its availability (generator produced) and cost-effectiveness, parameters important for routine clinical application. A folate derivative coupled with a hydrophobic N_3S chelator for ^{99m}Tc labelling, named ^{99m}Tc-EC20, developed by Leamon et al. and Reddy et al. [14, 15], has recently been used in a pilot study in patients with various solid tumours [23].

Nowadays positron emission tomography (PET) is becoming a dominating method in molecular imaging, since it combines the potential to quantify the tracer uptake within lesions with a relatively high resolution and a remarkably high sensitivity of up to 10^{-12} M. In combination with computed tomography (CT), providing anatomical information, hybrid instruments were developed that make the new technique PET/CT even more powerful. Among the β^+ emitters used for PET imaging, ^{68}Ga [$T_{1/2}$=67.71 min, $\overline{E}_{\beta^+}$ = 740 keV (89%)] deserves special attention. Its availability from long-lived ^{68}Ge/^{68}Ga generators, cost-effectiveness, rendering ^{68}Ga radiopharmacy possible in each hospital, well-established coordination chemistry of Ga^{3+} that allows developing agents resistant to in vivo transchelation of $^{68}Ga^{3+}$ and its suitable imaging properties make it attractive for clinical application [24, 25].

Folate conjugates for gallium complexation have been studied by the groups of Low and Green using deferoxamine (DF) as a chelator, since DF is known to form stable complexes with Ga^{3+} [26–29]. Studies were performed with ^{67}Ga for SPECT imaging [26–28] and more recently with ^{66}Ga for PET imaging [29]. The $^{66/67/68}$Ga-DF-folate conjugates showed good pharmacokinetics but also exhibited partial hepatobiliary clearance which is considered a limitation in cases of accurately imaging abdominal regions in humans, such as ovarian carcinoma. In order to overcome this obstacle the same group replaced DF with DTPA, which is ideal for labelling with ^{111}In [19, 20], but not with $^{67/68}$Ga. Indeed, ^{111}In-DTPA-folate showed a promising in vivo profile in animals, which led to clinical trials. This indicates the need for the development of new folate conjugates capable of being labelled with a variety of radionuclides, including $^{67/68}$Ga.

We have developed and evaluated two new ^{68}Ga-folate-based radiotracers. The chelator 1,4,7,10-tetraazacyclododecane-1,4,7,10-tetraacetic acid (DOTA), which is known to form stable complexes with Ga^{3+}, was attached to the folate moiety using two different spacers. The two new conjugates were labelled with $^{67/68}$Ga and preclinically evaluated in vitro and in vivo. For this purpose the KB cells (human nasopharyngeal carcinoma cell line) overexpressing the FR, which are most often used for the evaluation of FR-targeting agents, were used along with the HT1080 cells (human fibrosarcoma cell line), which were used as a negative control [30, 31]. Additionally, we compared our molecules with the "gold standard" folate-based SPECT radiotracer ^{111}In-DTPA-folate, which was synthesized and evaluated in parallel in all the assays and experiments of this study.

Materials and methods

General

All chemicals were obtained from commercial sources and used without further purification. $^{67}GaCl_3$ and $^{111}InCl_3$ were purchased from Mallinckrodt-Tyco (Petten, The Netherlands).

The $^{68}Ge/^{68}Ga$ generator was obtained from Cyclotron Co. Ltd. (Obninsk, Russia). Analytical reverse-phase high-performance liquid chromatography (RP-HPLC) was performed on a Hewlett Packard 1050 HPLC system (Waldbronn, Germany) with a multi-wavelength detector and a flow-through Berthold LB 506 C1 gamma detector using a Waters Symmetry C18 column (4.6×250 mm). The gradient system consisted of a mixture of water with 0.1% trifluoroacetic acid (TFA) (solvent A) and acetonitrile (solvent B), using the following gradient: 0–20 min, 95–80% A; 25 min, 80% A; 30 min, 50% A; 32 min, 95% A; 35 min, 95% A; at a flow rate of 0.75 ml/min. Electrospray ionization mass spectroscopy (ESI-MS) was performed on a Waters ZMD (Micromass) with an HP 1100 Quaternary LC pump. Quantitative gamma counting was performed on a COBRA 5003 gamma system well counter from Packard Instruments (Geneva, Switzerland). All reagents used in cell cultures were purchased from BioConcept (Allschwil, Switzerland).

Synthesis of the folate conjugates

The molecular formulas of the folate conjugates are shown in Fig. 1. The conjugates were synthesized in seven steps, using slightly modified published protocols [21]. A schematic representation of the synthetic route of P3026 is presented in Fig. 2.

Briefly, (a) a solution of di-*tert*-butyl (tBu) dicarbonate in dichloromethane (DCM) was added dropwise to 1,2-diaminoethane in a ratio of 1:4 and allowed to react for 2 h at room temperature (RT), followed by extraction with water. The organic layer was dried over Na_2SO_4 and the product was purified by flash chromatography. (b) 9-Fluorenylmethoxycarbonyl (Fmoc)-Glu-OtBu was coupled to (2-amino-ethyl)-carbamic acid *tert*-butyl ester (1) after activation with *N*-hydroxysuccinimide (NHS) using dicyclohexylcarbodiimine (DCC) as a coupling reagent. The reaction took place in DCM for 2 h at RT, followed by the same procedure described above for the isolation of the product. (c) The Fmoc group was removed with 20% piperidine in acetonitrile, under argon atmosphere, and the reaction mixture was evaporated and purified by flash chromatography. (d) Coupling of pteroic acid to 2-amino-4-(2-*tert*-butoxycarbonylamino-ethylcarbamoyl)-butyric acid *tert*-butyl ester (3) was performed in a ratio of 1:1 in dimethyl sulfoxide (DMSO) under argon atmosphere using 1-ethyl-3-(3-dimethylaminopropyl)carbodiimide (EDCI) as an activating reagent and hydroxybenzotriazole (HOBt) as a coupling reagent. The reaction mixture was incubated at 40°C overnight followed by precipitation in water. The residue was filtered and washed with water followed by diethyl ether. (e) The protecting groups were removed after treatment with TFA for 1 h at RT, followed by precipitation in diethyl ether. (f) The prochelator $DOTA(tBu)_3$ was dissolved in DCM and pre-activated for 30 min with NHS and DCC under argon atmosphere, followed by filtration of dicyclohexylurea. The solution of the activated ester was added to 4-(2-amino-ethylcarbamoyl)-2-{4-[(2-amino-4-oxo-3,4-dihydro-pteridin-6-ylmethyl)-amino]-benzoylamino}-butyric acid (5) (1:1.1 ratio) dissolved in DMSO along with 2 eq of triethylamine. After incubation for 1 h at RT the reaction mixture was precipitated in diethyl ether. The product obtained (6) was purified by flash chromatography. (g) The protecting groups were removed after treatment with TFA for 6 h at RT, followed by evaporation and precipitation in diethyl ether. The final product (7) was purified by preparative HPLC and identified by ESI-MS.

P1254 was obtained following the same synthetic route using 3-{2-[2-(3-amino-propoxy)-ethoxy]-ethoxy}-propyl-amine instead of 1,2-diaminoethane in the first step. P3139 was obtained by using the bisanhydride DTPA as described in the literature [19]. All conjugates were lyophilized after purification and characterized by HPLC and ESI-MS.

Preparation of the radiotracers

^{67}Ga-P3026, ^{67}Ga-P1254 and ^{111}In-P3139 were prepared by incubating 10 μg of each conjugate in 250 μl sodium acetate buffer 0.4 M, pH 5.0 with 37–74 MBq $^{67}GaCl_3$ or $^{111}InCl_3$ at 95°C for 30 min. $^{nat}Ga(NO_3)_3\times 9H_2O$ was used for the formation of the metal complexes ^{nat}Ga-P3026 and ^{nat}Ga-P1254, following the same protocol.

For the preparation of ^{68}Ga-P3026/P1254 a modified protocol of Zhernosekov et al. was followed [32]. Briefly, the $^{68}Ge/^{68}Ga$ generator was eluted with 7 ml HCl 0.1 N and the eluate was loaded onto a cation exchange column (strata-X-C, Phenomenex, Torrance, CA, USA). ^{68}Ga was eluted with 400 μl of a mixture of 97.6% acetone and 0.05 M HCl directly in a vial containing 400 μl 4-(2-hydroxyethyl)-1-piperazineethanesulfonic acid (HEPES) 0.25 M. The pH was controlled and adjusted in the range of 3.6–3.9, with HCl 0.1 M. Ten microlitres of P3026 or P1254 solution (2 mg/ml in H_2O) was then added and the reaction mixture was incubated at 95°C for 10 min.

Quality control was performed by RP-HPLC. The radiofolates were prepared by dilution with 0.9% NaCl (saline) with 0.1% bovine serum albumin (BSA). For the saturation binding studies $^{67/nat}Ga$-P3026 and $^{67/nat}Ga$-P1254, with tracer amounts of ^{67}Ga, were used to afford structurally characterized homogeneous compounds.

Cell cultures

The KB and HT1080 cell lines were obtained from American Type Culture Collection (ATCC, Manassas, VA, USA) (CCL-17 and CCL-21, respectively). The cells were

Folate conjugates	Chemical structure
P3026 $C_{37}H_{51}N_{13}O_{12}$ M.W. 869.90	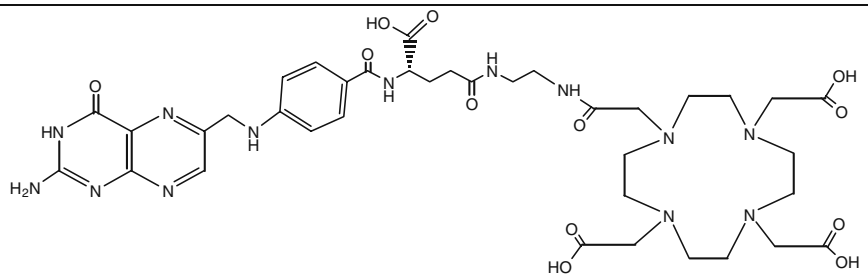
P1254 $C_{45}H_{67}N_{13}O_{15}$ M.W. 1030.11	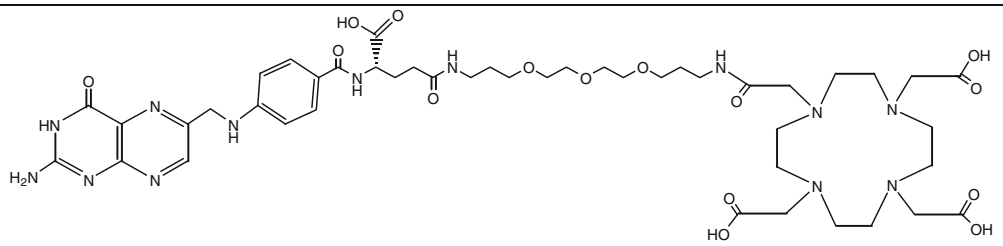
P3139 $C_{35}H_{46}N_{12}O_{14}$ M.W. 858.83	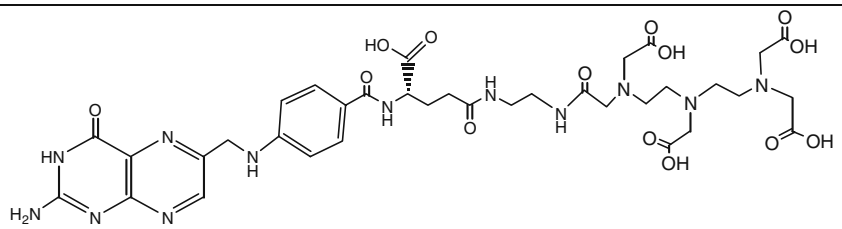

Fig. 1 Structures of the new DOTA-folate conjugates (P1254 and P3026) and of the reference molecule DTPA-folate (P3139)

cultured as monolayers at 37°C/5% CO_2 in folate-free RPMI 1640 medium (KB) and DMEM high-glucose (4.5 g/l) medium (HT1080). The media were supplemented with 10% fetal calf serum (FCS), L-glutamine and antibiotics (penicillin, 100 IU/ml; streptomycin, 100 μg/ml).

For the in vitro experiments the KB cells were seeded into 6-well plates ($0.8–1\times10^6$ cells/well) and incubated at 37°C/5% CO_2 overnight. On the day of the experiment the medium was removed, the cells were washed with RPMI medium without FCS and antibiotics and 800 μl/well pure medium were added. The plates were incubated at 37°C/5% CO_2 for 1 h. All experiments were performed in triplicate. For the in vivo experiments the cells were washed and suspended in sterile phosphate-buffered saline (PBS) at a concentration of 1×10^7 cells/ml.

Radiofolate cell uptake and internalization studies

For the internalization experiments 2.5 pmol/100 μl per well of each radiofolate was added and the cells were incubated at 37°C/5% CO_2 for preselected time points of 30 min, 1, 2 and 4 h at a final concentration of 2.5 nM. A 1,000-fold excess of folic acid (FA) was used to determine nonspecific binding and internalization. At the preselected time points the medium was removed, the cells were washed 2×1 ml PBS and were treated twice for 5 min with 1 ml ice-cold glycine solution (0.05 mol/l, pH 2.8) to distinguish between cell surface-bound (acid releasable) and internalized (acid resistant) radiofolate. Finally, the cells were detached by treatment with 1 ml of NaOH 1 N, followed by two washes. The radioactivity of all fractions was measured in the gamma counter. Receptor-specific internalization was calculated by subtracting the value found for blocked uptake from the total uptake and expressed as percentage of the applied radioactivity.

Externalization studies

The kinetics of externalization was studied after the cells were incubated for 2 h with 2.5 pmol/well. The medium was then removed and the cells were washed with 2×1 ml PBS and then exposed to an acid wash with glycine buffer, as described above, to dissociate cell surface-bound radiofolate. Pure medium (1 ml/well) was added and the cells were then incubated at 37°C. At different time points (15, 30, 60, 90, 120 and 240 min) the external medium was removed (followed by two washes with PBS) for quantification in a gamma counter and replaced with fresh 37°C medium. Finally, the cells were removed with NaOH 1 N and quantified in a gamma counter. The recycled fraction

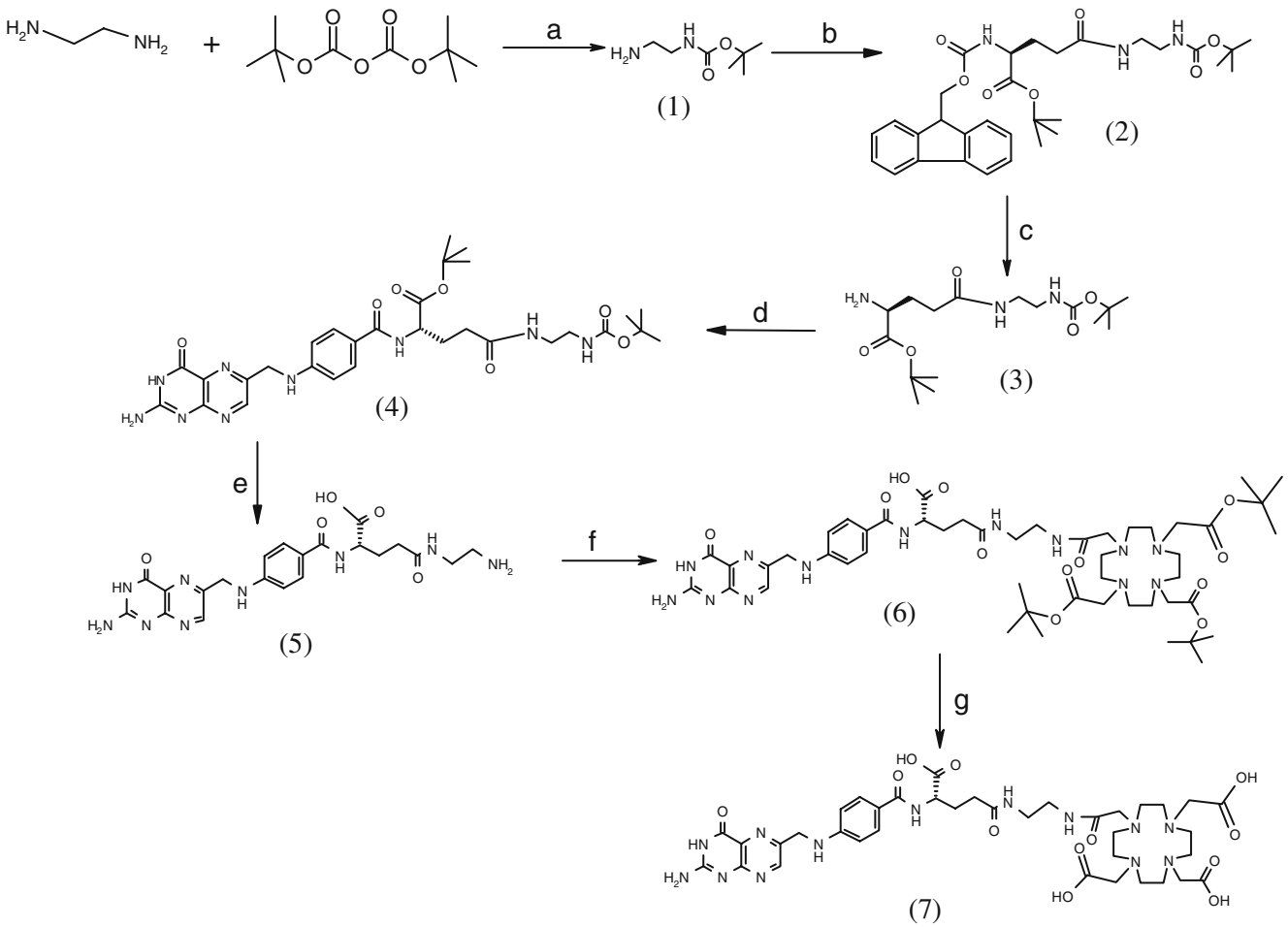

Fig. 2 Synthesis of P3026. **a** DCM; **b** Fmoc-Glu-OtBu, NHS/DCC, DCM; **c** 20% piperidine in acetonitrile; **d** pteroic acid, EDCI/HOBt, DMSO; **e** TFA; **f** DOTA(tBu)$_3$, NHS/DCC; **g** TFA

was expressed as the percentage of the total internalized amount.

Saturation binding assays

Increasing concentrations of $^{67/nat}$Ga-P1254 and $^{67/nat}$Ga-P3026, ranging from 0.1 to 1,000 nmol/l, were used for saturation binding experiments on intact cells. FA at a concentration of 1 mM was used to quantify the nonspecific binding. The cells were incubated for 2 h at 4°C in the presence of the radiofolates at different concentrations. The medium was removed and the cells were washed with 2×1 ml PBS; this represented the free fraction. The cells were collected with NaOH 1 N, which corresponded to the bound fraction. The radioactivity of both fractions was measured in a gamma counter. Dissociation constant (K_d) and maximum number of binding sites (B_{max}) values were calculated from the analysis of the data using GraphPad Prism 5.01 software (GraphPad Software Inc.).

Tumour model and animal biodistribution studies

All animal studies were performed in accordance with Swiss regulations (approval 789). Athymic female nude mice (4–5 weeks old, 18–20 g) were subcutaneously inoculated in the right front leg with 1×10^6 KB cells and in the other leg with 1×10^6 HT1080 cells. Tumours were allowed to grow for 9–10 days, when tumours were 68.6±22.7 mg and 99.8±56.2 mg for KB and HT1080, respectively. The animals stayed on a folate-deficient diet (semisynthetic product with 50 μg/kg of folate, S.A.F.E., Épinay-sur-Orge, France) 1 week before the implantation of the tumours until the end of the studies.

For the biodistribution studies the mice were divided into groups of between four and seven and injected with 0.4 nmol/1.5 MBq per 100 μl of each radiofolate into the tail vein. Nonspecific uptake in tumour and FR-positive organs was determined by 5 min pre-injection of 40 nmol FA/100 μl. At preselected time points of 20 min, 1, 2, 4 and 24 h post-injection (p.i.) the mice were sacrificed. The organs of interest

were collected, blotted dry, weighed and counted in a gamma counter. The results are expressed as the percentage of injected dose per gram (%ID/g ± SD) for each organ.

PET/CT images

For the PET/CT images the mice were injected intravenously with 0.4 nmol/4 MBq per 100 μl of ^{68}Ga-P3026. One hour later the mice were sacrificed, the kidneys were removed surgically and the mice were then scanned for 30 min using a routine combined PET/CT scanner (Discovery STE, GE Medical Systems, Waukesha, WI, USA). Images of mice pre-injected with FA, as described above, were also acquired. A scout scan (180°, 10 mA, 120 kV) was done to establish a protocol for all other scans. CT scans were acquired with minimum slice distance and the highest possible tube current for these settings (320 mA @ 120 keV). PET emission events were collected in 3-D scanning mode (septa out) over 30 min, starting immediately after the CT scan. They were corrected for decay of ^{68}Ga and random events and reconstructed using the manufacturer's 3-D ordered subset expectation maximization (OSEM) algorithm to 47 slices [display field of view (FOV)=6.4 cm, 128×128 matrix, resulting pixel size= 0.5 mm], once for each mouse separately in the centre of the reconstruction cylinder.

Statistical analysis

Student's *t* test was used to determine statistical significance. Differences at the 95% confidence level ($p<0.05$) were considered significant.

Results

Synthesis and radiolabelling

The synthetic strategy followed preserved the natural S configuration of the asymmetric carbon of the folate moiety and resulted selectively in the formation of the γ regioisomers. The overall yield of synthesis was ~10%. All conjugates were obtained in 92–95% purity, as confirmed by RP-HPLC. The observed mass in ESI-MS was: 893.2 $[M+Na]^+$ for P3026, 1,068.9 $[M+K]^+$ for P1254 and 859.7 $[M+H]^+$ for P3139. The radiofolates were prepared in a labelling yield of>95%. Specific activity of the ^{67}Ga- and ^{68}Ga-DOTA-folate conjugates was at the level of 7 and 10 MBq/nmol, respectively.

Cell uptake, internalization and externalization studies

All radiofolates are highly and rapidly associated with the KB cells within the initial 30 min of incubation. Figure 3 shows the cell uptake and retention of the radiofolates into KB cells over time. Continued exposure of the cells to the radiofolates resulted in a slight increase of uptake from 30 min to 4 h, which was more obvious in the case of ^{67}Ga-P3026. ^{67}Ga-P3026 was found to have the highest cell-associated uptake (80%) and the highest cell surface binding value (63.9±1.2%), compared to ^{67}Ga-P1254 and ^{111}In-P3139 (55.7±1.5% and 49.6±2.5%, respectively), at 4 h. The internalized fraction increased with time, from 30 min to 4 h. The highest value was found for ^{67}Ga-P3026 (16.5±0.4%), while for the other radiofolates this value ranged from 9.5 to 12%. Blocking experiments performed with excess of FA showed negligible nonspecific binding on the cell surface, while less than 0.5% of total added radioactivity was found to be internalized (data not shown). These results demonstrate the high specificity of the folate conjugates for the FRs in vitro. As far as the externalization concerns, ^{67}Ga-P1254 showed the highest retention in the cells (82% retained in the cells after 4 h at 37°C). Comparable values were found for ^{67}Ga-P3026, while for ^{111}In-P3139 up to 40% was found to be released from the cells into the medium.

Saturation binding studies

Saturation binding studies were performed at 4°C, in order to allow binding of the radiofolates to the receptor but to avoid endocytosis. The results are presented in Fig. 4. Both $^{67/nat}$Ga-DOTA-folates exhibited the same affinity for the FR, with K_d values of 4.65±0.82 nM for $^{67/nat}$Ga-P3026 and 4.27±0.42 nM for $^{67/nat}$Ga-P1254. The B_{max} values were also at the same level for both conjugates (10.65±0.45 nM for $^{67/nat}$Ga-P3026 and 11.44±0.27 nM for $^{67/nat}$Ga-P1254). A number of approximately 6.4 to 6.9×10^6 molecules of $^{67/nat}$Ga-DOTA-folates was estimated to be associated with each KB cell when maximum binding was achieved.

Biodistribution studies

Biodistribution studies of all radiofolates were performed in a dual tumour model of nude mice bearing FR-positive KB tumours and FR-negative HT1080 tumours from 20 min up to 24 h p.i. The biodistribution profile of all radiofolates is characterized by efficient clearance from the blood, high and specific receptor-mediated tumour uptake and high radioactivity accumulation in the kidneys. The results are summarized in Tables 1, 2 and 3.

The uptake in the FR-positive tumour was found to be high from the earliest time point of the study (20 min p.i.), having similar maximum values for all conjugates at 4 h p.i. ($^{67/68}$Ga-P3026: 14.29±4.14%ID/g, $^{67/68}$Ga-P1254: 13.10± 0.65%ID/g and ^{111}In-P3139: 12.13±2.16%ID/g). However,

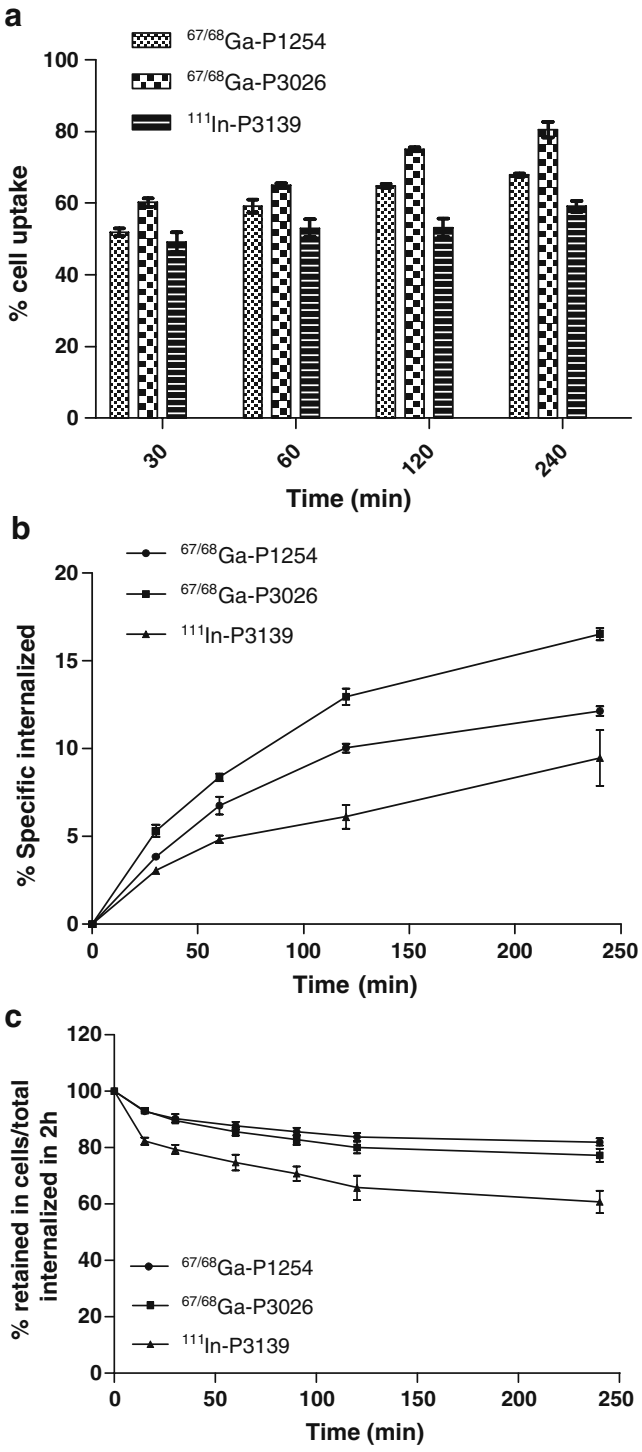

Fig. 3 Time-dependent cell uptake and retention of ^{67}Ga-P3026, ^{67}Ga-P1254 and ^{111}In-3139 into KB cells (1×10^6 cells/2.5 pmol per ml), within 4 h at 37°C. **a** Cell uptake calculated as cell surface-bound and internalized fraction. **b** Receptor-specific internalization expressed as percentage of the applied radioactivity. **c** Cellular retention expressed as the percentage that remained in the cells from the total amount internalized (100%). All data are from three independent experiments with triplicates in each experiment

the difference in the tumour uptake was not significant from 1 to 4 h p.i. ($p>0.05$). A slow washout from the tumour occurred, as the values were still high 24 h p.i. As was expected kidneys accumulated high amounts of radioactivity and as a consequence tumour to kidney ratios were low at all investigated time points. In all cases, the radioactivity concentration in the FR-negative HT1080 tumours was much lower, around 1–2%ID/g. The specificity of the conjugates for the FR was also confirmed by blocking experiments in which tumour and kidney uptake were drastically reduced when FA was pre-injected.

Focusing on the tumour to non-tumour ratios, all values were already high at 1 h p.i. (tumour to blood: ~40, tumour to liver: ~2.5, tumour to muscles: 5–10) and increased with time. This was not the case for the tumour to kidney ratios which were low and remained essentially the same from 20 min up to 4 h p.i. Among the conjugates ^{111}In-P3139 seemed to have a slightly better tumour to kidney ratio but

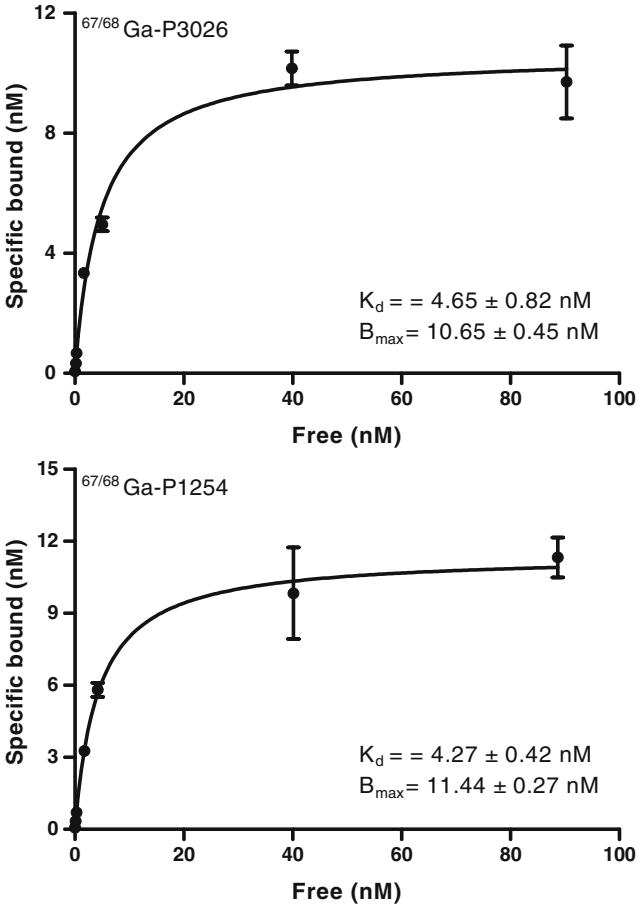

Fig. 4 Saturation binding study on intact KB cells, using increased concentrations of $^{67/nat}$Ga-P3026 and $^{67/nat}$Ga-P1254, ranging from 0.1 to 1,000 nM. Dissociation constant (K_d) and maximum number of binding sites (B_{max}) were calculated from nonlinear regression analysis using GraphPad Prism. All data are from three independent experiments with triplicates in each experiment

Table 1 Biodistribution results (%ID/g ± SD, n=4–7) and tumour to non-tumour ratios of $^{67/68}$Ga-P3026 in nude mice bearing KB and HT1080 tumours

Organ	20 min	1 h	2 h	4 h	4 h blocking	24 h
Blood	0.94±0.25	0.32±0.03	0.21±0.01	0.20±0.04	0.09±0.02	0.08±0.01
Heart	3.74±0.39	3.24±0.23	2.99±0.26	2.54±0.21	0.06±0.01	2.55±0.29
Liver	7.62±1.75	4.88±0.81	2.92±0.48	2.08±0.08	0.14±0.04	2.28±0.22
Spleen	0.59±0.09	0.60±0.07	0.55±0.16	0.60±0.22	0.08±0.01	0.44±0.06
Lung	2.35±0.74	1.99±0.21	1.73±0.33	1.47±0.27	0.11±0.02	1.10±0.23
Kidney	62.90±11.57	82.21±5.53	87.78±12.37	103.01±24.58	6.36±1.13	95.67±11.37
Stomach	2.66±0.56	2.12±0.14	1.95±0.11	1.66±0.18	0.08±0.02	1.60±0.21
Intestine	0.92±0.13	0.65±0.19	0.68±0.13	0.82±0.18	0.09±0.02	0.77±0.20
Adrenal	5.77±0.74	4.63±0.95	3.79±0.57	3.21±0.40	0.13±0.05	2.54±0.68
Pancreas	4.85±0.28	4.69±0.16	3.86±0.55	3.26±0.43	0.07±0.02	2.67±0.33
Pituitary	1.73±0.24	3.57±0.55	2.09±0.78	2.32±0.42	0.11±0.01	1.79±0.16
Muscle	2.12±0.57	2.19±0.21	2.25±0.43	1.70±0.32	0.03±0.01	1.28±0.08
Bone	0.53±0.21	0.47±0.14	0.44±0.09	0.37±0.13	0.08±0.02	0.51±0.05
KB tumour	8.82±1.59	11.77±2.76	10.64±2.13	14.29±4.14	2.39±0.71	7.36±1.37
HT1080 tumour	1.78±0.76	1.16±0.65	1.48±0.91	1.04±0.52	0.09±0.02	0.48±0.05
Tumour to non-tumour ratios						
Tumour to blood	9.91±3.18	36.19±5.05	50.12±11.21	70.01±7.37		90.11±18.18
Tumour to liver	1.12±0.35	2.62±0.72	4.07±1.30	6.88±2.08		3.27±0.75
Tumour to muscles	4.40±1.37	5.39±1.20	4.84±1.21	8.87±3.78		5.73±0.91
Tumour to kidneys	0.14±0.03	0.14±0.04	0.12±0.02	0.12±0.01		0.08±0.01

Table 2 Biodistribution results (%ID/g ± SD, n=4–7) and tumour to non-tumour ratios of $^{67/68}$Ga-P1254 in nude mice bearing KB and HT1080 tumours

Organ	20 min	1 h	2 h	4 h	4 h blocking	24 h
Blood	0.84±0.12	0.32±0.02	0.26±0.03	0.21±0.01	0.12±0.01	0.07±0.01
Heart	2.04±0.24	1.96±0.14	1.90±0.22	1.94±0.15	0.06±0.01	1.67±0.22
Liver	8.80±1.08	5.48±1.13	3.68±0.95	2.24±0.17	0.20±0.02	2.40±0.82
Spleen	0.58±0.19	0.45±0.09	0.54±0.12	0.46±0.06	0.11±0.01	0.35±0.06
Lung	1.86±0.50	1.30±0.22	1.40±0.27	1.30±0.20	0.18±0.03	0.89±0.11
Kidney	79.32±14.08	84.85±13.69	98.43±15.40	103.95±16.96	3.48±0.70	93.95±11.13
Stomach	1.82±0.11	1.45±0.15	1.54±0.19	1.60±0.13	0.09±0.01	1.12±0.19
Intestine	0.69±0.09	0.54±0.08	0.49±0.09	0.62±0.05	0.14±0.02	0.73±0.19
Adrenal	6.54±1.06	4.05±1.04	4.37±0.81	2.99±0.30	0.16±0.05	2.26±0.60
Pancreas	3.14±0.16	2.75±0.32	2.68±0.37	2.80±0.28	0.06±0.01	2.25±0.39
Pituitary	2.02±0.37	2.47±0.17	2.30±0.57	1.65±0.85	0.07±0.04	0.73±0.30
Muscle	1.43±0.13	1.37±0.46	1.32±0.21	1.44±0.33	0.03±0.01	1.07±0.02
Bone	0.64±0.35	0.25±0.04	0.20±0.07	0.26±0.04	0.09±0.01	0.28±0.05
KB tumour	8.87±1.06	12.51±1.54	10.37±0.36	13.10±0.65	0.81±0.17	7.41±1.49
HT1080 tumour	1.39±0.87	1.43±0.91	2.36±0.15	1.26±0.53	0.09±0.01	1.49±0.75
Tumour to non-tumour ratios						
Tumour to blood	10.73±1.67	39.27±2.35	40.80±2.07	63.00±2.75		102.34±19.04
Tumour to liver	1.03±0.23	2.35±0.53	2.91±0.78	5.89±0.66		3.23±0.72
Tumour to muscles	6.27±1.21	9.57±1.70	8.48±1.25	9.37±1.55		6.94±1.34
Tumour to kidneys	0.11±0.02	0.15±0.01	0.11±0.02	0.13±0.03		0.08±0.01

Table 3 Biodistribution results (%ID/g ± SD, n=4–7) and tumour to non-tumour ratios of ^{111}In-P3139 in nude mice bearing KB and HT1080 tumours

Organ	20 min	1 h	2 h	4 h	4 h blocking	24 h
Blood	0.81±0.19	0.24±0.02	0.17±0.04	0.10±0.02	0.01±0.00	0.08±0.02
Heart	4.62±0.63	4.32±0.76	3.65±0.37	3.08±0.26	0.01±0.01	2.24±0.55
Liver	7.49±1.11	4.19±1.71	2.29±0.70	1.52±0.23	0.04±0.01	0.98±0.24
Spleen	0.72±0.14	0.62±0.15	0.57±0.08	0.61±0.14	0.04±0.01	0.63±0.21
Lung	2.28±0.20	1.86±0.17	1.97±0.30	1.77±0.31	0.05±0.01	1.46±0.32
Kidney	55.97±7.99	67.32±11.07	68.78±6.72	77.09±10.67	2.97±0.43	72.81±15.61
Stomach	2.34±0.33	1.95±0.31	1.94±0.33	2.04±0.33	0.04±0.01	1.38±0.27
Intestine	1.06±0.43	0.87±0.11	0.80±0.10	0.61±0.19	0.03±0.01	0.56±0.06
Adrenal	4.93±1.13	3.77±0.91	3.03±0.50	3.24±0.46	0.08±0.03	2.30±0.38
Pancreas	4.77±0.76	3.42±0.43	4.00±0.94	3.46±0.54	0.02±0.01	2.47±0.34
Pituitary	3.55±0.84	3.91±0.20	3.54±0.87	3.25±0.61	0.03±0.02	3.36±0.50
Muscle	2.41±0.09	2.40±0.48	2.16±0.34	1.80±0.22	0.01±0.01	1.36±0.03
Bone	0.61±0.04	0.42±0.13	0.46±0.12	0.56±0.23	0.04±0.02	0.56±0.22
KB tumour	9.66±1.09	11.11±1.51	12.46±0.77	12.13±2.16	0.61±0.21	10.64±3.67
HT1080 tumour	1.80±0.55	2.01±0.83	0.91±0.57	0.86±0.45	0.04±0.01	0.62±0.18
Tumour to non-tumour ratios						
Tumour to blood	12.34±2.51	46.11±8.54	76.30±16.53	118.07±22.28		131.76±30.70
Tumour to liver	1.30±0.17	2.98±1.18	5.76±1.45	8.19±2.13		11.77±5.92
Tumour to muscles	4.01±0.43	4.70±0.67	5.84±0.73	6.91±2.14		7.79±2.58
Tumour to kidneys	0.17±0.03	0.17±0.01	0.18±0.02	0.16±0.01		0.12±0.01

it was found to be statistically not significant, compared to $^{67/68}$Ga-DOTA-folates (p>0.05).

PET/CT images

PET/CT images were performed with ^{68}Ga-P3026 at 1 h p.i. For this study the kidneys were surgically removed from the mice before imaging, in order to localize the tumour, since kidneys accumulate high amounts of radioactivity. The PET/CT images (Fig. 5) clearly showed high and specific uptake of ^{68}Ga-P3026 in the FR-positive tumour and negligible uptake in the FR-negative tumour, with very good tumour to non-tumour contrast. The PET/CT images of mice pre-injected with FA, where kidneys had not been removed, confirmed the specificity of the radiofolate for the FR. High uptake was also observed in the salivary glands, which was negligible in the case of FA pre-injection, demonstrating the receptor-mediated uptake of the radiofolate by this tissue.

Discussion

Ovarian cancer at its early stages is difficult to diagnose until it spreads and advances to later stages. Since metastatic spreading is a negative prognostic factor for survival there is an acute need for a diagnostic tool allowing early detection. The folate receptor can be used as a tumour-associated molecular target in this case since it is highly expressed in ovarian and endometrial carcinomas. On the other hand, a rational design and development of a selective and specific PET radiotracer for this target gives the chance of using the advantages of PET/CT technology for early detection, staging and follow-up of patients suffering from ovarian cancer. Moreover, it will provide information on the presence or absence of the molecular target, which is extremely important for the design and implementation of therapeutic approaches.

Based on the above rationale we designed and developed PET folate-based radiotracers, using the generator-produced ^{68}Ga, which would make the preparation of the radiopharmaceutical possible in every hospital. We chose DOTA as a chelator and conjugated it to folic acid using different spacer molecules as potential pharmacokinetic modifiers, such as 1,2-diaminoethane and 3-{2-[2-(3-amino-propoxy)-ethoxy]-ethoxy}-propylamine, resulting in the conjugates P3026 and P1254, respectively. Folic acid has two carboxylic acid groups (α and γ) available for coupling. It is still unclear whether a free α carboxyl group is necessary for folate conjugates to retain binding to the FR. As there is some debate on the affinity of the α regioisomer, while the γ regioisomer is known to have high affinity for the FR [19, 33, 34], we followed the synthetic strategy described in the "Materials and methods"

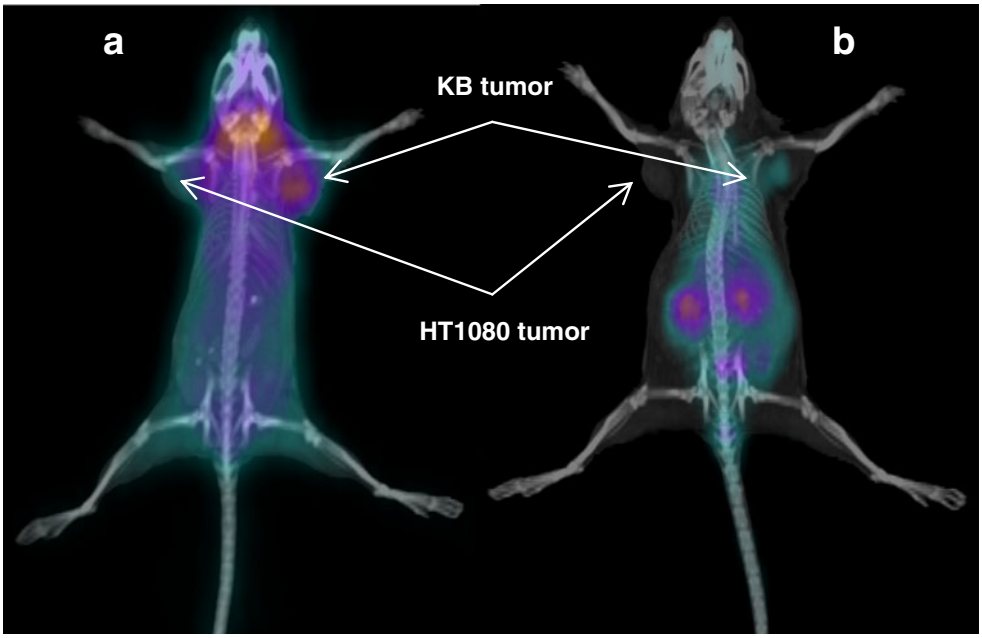

Fig. 5 PET/CT images 1 h p.i. of ^{68}Ga-P3026 (**a**), where specific uptake in the KB tumour (FR+), but also in the salivary glands, was observed, while no uptake in the HT1080 tumour (FR-) was observed. In this mouse the kidneys were removed prior to imaging due to the high kidney uptake of the folate derivatives. **b** ^{68}Ga-P3026 co-injected with folic acid (100-fold excess) demonstrated the specific uptake of the radiotracer, since reduced kidney uptake and negligible tumour uptake in the FR+tumour was observed

section to obtain the selective γ regioisomers of our conjugates. The DOTA-folate conjugates were labelled with ^{67}Ga ($T_{1/2}$=3.26 days), which gives the possibility of investigations at late time points. The $^{67/68}$Ga-DOTA-folates were preclinically evaluated along with the ^{111}In-DTPA-folate (^{111}In-P3139), which was used as a reference molecule [19, 20, 22, 35].

All of the conjugates exhibit a rapid FR association in vitro, with the $^{67/68}$Ga-P3026 and $^{67/68}$Ga-P1254 showing higher cell surface binding activity and internalization rate, compared to ^{111}In-P3139. It is worth mentioning that $^{67/68}$Ga-P3026 showed the highest cell-associated uptake, reaching 80% of the total added activity, at 4 h, compared to 60% found for ^{111}In-P3139 under the same experimental conditions and also to 40–60% published for different radiofolates and cell lines, including KB cells [16, 30, 36]. A twofold higher cellular retention was observed for the $^{67/68}$Ga-P3026 and $^{67/68}$Ga-P1254, compared to ^{111}In-P3139. The retention of the radiofolates in the cells may be an important parameter for potential use of these conjugates in therapeutic applications, as cellular retention determines the radiation dose deposited in the tumour [37].

$^{67/68}$Ga-P3026 and $^{67/68}$Ga-P1254 exhibited high affinity for the FR with K_d values in the low nanomolar range, comparable to folic acid [1, 16, 30], while the maximum number of molecules associated per KB cell is in agreement with the literature [14, 26, 36].

The two new $^{67/68}$Ga-DOTA-folates target selectively FR-expressing tumours in vivo, with very high tumour to non-tumour contrast, except the kidneys where filtration of folates and reabsorption from the primary urine via the FR in proximal tubules leads to high retention of radioactivity. To our knowledge, there is only one folate conjugate (DF-folate) which has been studied with $^{66/67/68}$Ga and PET images have been acquired with ^{66}Ga [29], while no ^{68}Ga has been used for PET imaging with folate derivatives. Despite the good pharmacokinetics of the $^{66/67}$Ga-DF-folate conjugate and its primary excretion via urine, > 20% is cleared via intestines 4 h p.i. [27, 28] which is a drawback since radioactivity will interfere with imaging of abdominal tumours, such as ovarian carcinoma. The $^{67/68}$Ga-DOTA-folates showed better pharmacokinetics compared to $^{66/67}$Ga-DF-folate with efficient clearance from the blood, elimination via the kidneys and high and specific receptor-mediated tumour uptake, while no significant amount of radioactivity is concentrated in the gastrointestinal track.

The biodistribution profile of the $^{67/68}$Ga-DOTA-folates is similar to the reference molecule ^{111}In-P3139 in a side-by-side comparison, as it is known that parameters such as tumour size, serum folate concentration, folate conjugate structure and administered dose can affect the in vivo results [20, 28, 35, 38]. Among $^{67/68}$Ga-P3026, $^{67/68}$Ga-P1254 and ^{111}In-P3139, tumour uptake, kidney uptake and also tumour to kidney ratio, at 1 and 4 h p.i., were at the same level, with differences statistically not significant (p>0.05). This shows that the replacement of DTPA by DOTA (P3139 vs P3026), but also the replacement of the spacer (P1254 vs P3026), did not alter the biodistribution profile. However, this was not the case when the chelator DF was replaced by DTPA (DF-folate vs P3139). The difference in the in vivo behaviour of ^{67}Ga-DF-folate, compared to ^{111}In-P3139, $^{67/68}$Ga-P3026 and $^{67/68}$Ga-P1254, is possibly due to the dissociation of the metal, rather than the chelator and/or the spacer used, as there are indications that in nanomolar concentrations the stability of the Ga-DF complex may be reduced [39].

The clear visualization of the FR-positive tumours with PET/CT images of ^{68}Ga-P3026 proved the potency of these radiotracers to localize and detect tumours expressing the FR. We used a somewhat unusual way to eliminate the intensive signal received from the kidneys, by removing the kidneys surgically. Müller et al. have introduced the use of the antifolate pemetrexed for the elimination of the radiofolates concentrated in the kidneys [35]. It has also been shown that manipulation of the radiofolate uptake in the kidney, tumour and normal tissues, as well as in tumour to non-target contrast, can be achieved with co-administration of modest doses of folic acid [20, 28]. However, for the purpose of our study, no effort was made for such an optimization. Except the high and specific tumour uptake, confirmed by blocking experiments, PET/CT images demonstrated also high uptake in the salivary glands. The specific uptake of radiofolates in this tissue has recently been demonstrated with SPECT/CT imaging [17], while in the past no evidence of such an uptake was available. In addition, one should not forget that in the animal model the mice are on a folate-deficient diet. Interestingly, when we injected the radiofolates into non-tumour-bearing mice, without being on a folate-deficient diet, no uptake was found in the salivary glands on PET/CT images where only kidneys were visualized 1 h p.i. (data not shown). Obviously, this finding needs further investigation, as we do not really know how it reflects the human situation. Moreover, such an uptake has not been found in patients studied with radiofolates [22, 23].

The new $^{67/68}$Ga-DOTA-folate conjugates showed better pharmacokinetics, compared to $^{66/67/68}$Ga-DF-folate and similar to the clinically evaluated ^{111}In-DTPA-folate. ^{111}In-DTPA-folate scintigraphy in phase I/II clinical trials for imaging ovarian cancer showed that differentiation between benign and malignant masses was possible in patients with suspected new disease [22]. No significant uptake in any organ except kidney and tumour was observed and good contrast was achieved within 1 h suggesting that short-lived radionuclides, such as ^{68}Ga, can be exploited for imaging applications [22, 40]. Additionally, ^{99m}Tc-EC20 scintigraphy in patients with different solid tumours allowed FRs to be identified in recurrent or metastatic disease [23, 40]. In these clinical applications both radiofolates were shown to be safe. Single-dose intravenous injection was well tolerated in humans; no serious adverse reactions or changes in vital signs have been reported. Accordingly, in our preclinical evaluation no pharmacological side effects were observed in any group of animals.

At the beginning of our study no published data on DOTA-folate conjugates were available. Meanwhile two groups have presented their data based on similar conjugates in the concept of a therapeutic approach, either by using radionuclides such as ^{177}Lu [38] or by investigating ^{nat}Ga(III) compounds as anticancer agents [33], while DOTA conjugated to a monoclonal antibody has also been used for radioimmunotargeting of FR [41]. Their and our encouraging results make us believe that the development of these DOTA-folate conjugates has a positive impact on the folate receptor-targeted imaging and/or therapy. The high kidney uptake is a major concern, but for diagnostics it is not such a serious drawback as in the case of therapeutic radiopharmaceuticals, especially when PET isotopes with a short half-life are used. Moreover, preclinical studies for modulation of kidney radiotracer uptake with antifolates are ongoing [35, 38]. We also consider the use of ^{68}Ga preferable to ^{66}Ga for PET imaging, as far as dosimetry and availability are concerned.

In summary, two new DOTA-folate conjugates were developed and efficiently labelled with ^{68}Ga in labelling yields and specific activities which allow clinical application. High and selective targeting of FR along with good tumour to background ratio at early time points after injection can be achieved, showing the potentiality of these compounds as PET radiotracers for FR-positive tumours. The characteristics of the $^{67/68}$Ga-DOTA-folate conjugates are comparable to ^{111}In-DTPA-folate, which has already been used in clinical trials. This new development gives an option to improve the existing strategies of detection and treatment of FR-positive tumours, such as ovarian carcinoma.

Acknowledgements We thank the staff of the Division of Radiological Chemistry and the Department of Nuclear Medicine, University Hospital Basel, for their assistance. This work was supported by a research grant from Guerbet (Aulnay-sous-Bois, France). C. Medina, I. Raynal and M. Rort are employees of Guerbet. M. Fani, X. Wang, G. Nicolas and H.R. Maecke declare that they have no conflict of interest.

References

1. Antony AC. The biological chemistry of folate receptors. Blood 1992;79:2807–20.
2. Ross JF, Chaudhuri PK, Ratnam M. Differential regulation of folate receptor isoforms in normal and malignant tissues in vivo and in established cell lines. Physiologic and clinical implications. Cancer 1994;73:2432–43.
3. Antony AC. Folate receptors. Annu Rev Nutr 1996;16:501–21.
4. Toffoli G, Cernigoi C, Russo A, Gallo A, Bagnoli M, Boiocchi M. Overexpression of folate binding protein in ovarian cancers. Int J Cancer 1997;74:193–8.
5. Parker N, Turk MJ, Westrick E, Lewis JD, Low PS, Leamon CP. Folate receptor expression in carcinomas and normal tissues determined by a quantitative radioligand binding assay. Anal Biochem 2005;338:284–93.
6. Leamon CP, Low PS. Folate-mediated targeting: from diagnostics to drug and gene delivery. Drug Discov Today 2001;6:44–51.
7. Reddy JA, Allagadda VM, Leamon CP. Targeting therapeutic and imaging agents to folate receptor positive tumors. Curr Pharm Biotechnol 2005;6:131–50.

8. Salazar MD, Ratnam M. The folate receptor: what does it promise in tissue-targeted therapeutics? Cancer Metastasis Rev 2007; 26:141–52.
9. Low PS, Henne WA, Doorneweerd DD. Discovery and development of folic-acid-based receptor targeting for imaging and therapy of cancer and inflammatory diseases. Acc Chem Res 2008;41:120–9.
10. Leamon CP, Low PS. Delivery of macromolecules into living cells: a method that exploits folate receptor endocytosis. Proc Natl Acad Sci U S A 1991;88:5572–6.
11. Sabharanjak S, Mayor S. Folate receptor endocytosis and trafficking. Adv Drug Deliv Rev 2004;56:1099–109.
12. Guo W, Hinkle GH, Lee RJ. ^{99m}Tc-HYNIC-folate: a novel receptor-based targeted radiopharmaceutical for tumor imaging. J Nucl Med 1999;40:1563–9.
13. Mathias CJ, Hubers D, Low PS, Green MA. Synthesis of [(99 m) Tc]DTPA-folate and its evaluation as a folate-receptor-targeted radiopharmaceutical. Bioconjug Chem 2000;11:253–7.
14. Leamon CP, Parker MA, Vlahov IR, Xu LC, Reddy JA, Vetzel M, et al. Synthesis and biological evaluation of EC20: a new folate-derived, (99m)Tc-based radiopharmaceutical. Bioconjug Chem 2002;13:1200–10.
15. Reddy JA, Xu LC, Parker N, Vetzel M, Leamon CP. Preclinical evaluation of (99m)Tc-EC20 for imaging folate receptor-positive tumors. J Nucl Med 2004;45:857–66.
16. Müller C, Hohn A, Schubiger PA, Schibli R. Preclinical evaluation of novel organometallic ^{99m}Tc-folate and ^{99m}Tc-pteroate radiotracers for folate receptor-positive tumour targeting. Eur J Nucl Med Mol Imaging 2006;33:1007–16.
17. Müller C, Forrer F, Schibli R, Krenning EP, de Jong M. SPECT study of folate receptor-positive malignant and normal tissues in mice using a novel ^{99m}Tc-radiofolate. J Nucl Med 2008;49:310–7.
18. Mindt TL, Müller C, Melis M, de Jong M, Schibli R. "Click-to-chelate": in vitro and in vivo comparison of a ^{99m}Tc(CO)3-labeled N (tau)-histidine folate derivative with its isostructural, clicked 1,2,3-triazole analogue. Bioconjug Chem 2008;19:1689–95.
19. Wang S, Luo J, Lantrip DA, Waters DJ, Mathias CJ, Green MA, et al. Design and synthesis of [^{111}In]DTPA-folate for use as a tumor-targeted radiopharmaceutical. Bioconjug Chem 1997;8:673–9.
20. Mathias CJ, Wang S, Waters DJ, Turek JJ, Low PS, Green MA. Indium-111-DTPA-folate as a potential folate-receptor-targeted radiopharmaceutical. J Nucl Med 1998;39:1579–85.
21. Ke CY, Mathias CJ, Green MA. Targeting the tumor-associated folate receptor with an ^{111}In-DTPA conjugate of pteroic acid. J Am Chem Soc 2005;127:7421–6.
22. Siegel BA, Dehdashti F, Mutch DG, Podoloff DA, Wendt R, Sutton GP, et al. Evaluation of ^{111}In-DTPA-folate as a receptor-targeted diagnostic agent for ovarian cancer: initial clinical results. J Nucl Med 2003;44:700–7.
23. Fisher RE, Siegel BA, Edell SL, Oyesiku NM, Morgenstern DE, Messmann RA, et al. Exploratory study of ^{99m}Tc-EC20 imaging for identifying patients with folate receptor-positive solid tumors. J Nucl Med 2008;49:899–906.
24. Al-Nahhas A, Win Z, Szyszko T, Singh A, Nanni C, Fanti S, et al. Gallium-68 PET: a new frontier in receptor cancer imaging. Anticancer Res 2007;27:4087–94.
25. Fani M, André JP, Maecke HR. ^{68}Ga-PET: a powerful generator-based alternative to cyclotron-based PET radiopharmaceuticals. Contrast Media Mol Imaging 2008;3:67–77.
26. Wang S, Lee RJ, Mathias CJ, Green MA, Low PS. Synthesis, purification, and tumor cell uptake of ^{67}Ga-deferoxamine–folate, a potential radiopharmaceutical for tumor imaging. Bioconjug Chem 1996;7:56–62.
27. Mathias CJ, Wang S, Lee RJ, Waters DJ, Low PS, Green MA. Tumor-selective radiopharmaceutical targeting via receptor-mediated endocytosis of gallium-67-deferoxamine-folate. J Nucl Med 1996;37:1003–8.
28. Mathias CJ, Wang S, Low PS, Waters DJ, Green MA. Receptor-mediated targeting of ^{67}Ga-deferoxamine-folate to folate-receptor-positive human KB tumor xenografts. Nucl Med Biol 1999;26:23–5.
29. Mathias CJ, Lewis MR, Reichert DE, Laforest R, Sharp TL, Lewis JS, et al. Preparation of ^{66}Ga- and ^{68}Ga-labeled Ga(III)-deferoxamine-folate as potential folate-receptor-targeted PET radiopharmaceuticals. Nucl Med Biol 2003;30:725–31.
30. Müller C, Schubiger PA, Schibli R. In vitro and in vivo targeting of different folate receptor-positive cancer cell lines with a novel ^{99m}Tc-radiofolate tracer. Eur J Nucl Med Mol Imaging 2006;33:1162–70.
31. Campbell IG, Jones TA, Foulkes WD, Trowsdale J. Folate-binding protein is a marker for ovarian cancer. Cancer Res 1991;51:5329–38.
32. Zhernosekov KP, Filosofov DV, Baum RP, Aschoff P, Bihl H, Razbash AA, et al. Processing of generator-produced ^{68}Ga for medical application. J Nucl Med 2007;48:1741–8.
33. Viola-Villegas N, Vortherms A, Doyle RP. Targeting gallium to cancer cells through the folate receptor. Drug Target Insights 2008;3:13–25.
34. Ross TL, Honer M, Lam PY, Mindt TL, Groehn V, Schibli R, et al. Fluorine-18 click radiosynthesis and preclinical evaluation of a new ^{18}F-labeled folic acid derivative. Bioconjug Chem 2008;19:2462–70.
35. Müller C, Schibli R, Krenning EP, de Jong M. Pemetrexed improves tumor selectivity of ^{111}In-DTPA-folate in mice with folate receptor-positive ovarian cancer. J Nucl Med 2008;49:623–9.
36. Paulos CM, Reddy JA, Leamon CP, Turk MJ, Low PS. Ligand binding and kinetics of folate receptor recycling in vivo: impact on receptor-mediated drug delivery. Mol Pharmacol 2004;66:1406–14.
37. Ginj M, Zhang H, Eisenwiener KP, Wild D, Schulz S, Rink H, et al. New pansomatostatin ligands and their chelated versions: affinity profile, agonist activity, internalization, and tumor targeting. Clin Cancer Res 2008;14:2019–27.
38. Müller C, Mindt TL, de Jong M, Schibli R. Evaluation of a novel radiofolate in tumour-bearing mice: promising prospects for folate-based radionuclide therapy. Eur J Nucl Med Mol Imaging 2009;36:938–46.
39. Caraco C, Aloj L, Eckelman WC. The gallium-deferoxamine complex: stability with different deferoxamine concentrations and incubation conditions. Appl Radiat Isot 1998;49:1477–9.
40. Sega EI, Low PS. Tumor detection using folate receptor-targeted imaging agents. Cancer Metastasis Rev 2008;27:655–64.
41. Smith-Jones PM, Pandit-Taskar N, Cao W, O'Donoghue J, Philips MD, Carrasquillo J, et al. Preclinical radioimmunotargeting of folate receptor alpha using the monoclonal antibody conjugate DOTA-MORAb-003. Nucl Med Biol 2008;35:343–51.